Applying twisted boundary conditions for few-body nuclear systems

Christopher Körber and Thomas Luu
Institute for Advanced Simulations 4, Institut für Kernphysik 3, Forschungszentrum Jülich, D-52425 Jülich, Germany
(Received 9 December 2015; revised manuscript received 6 March 2016; published 19 May 2016)

We describe and implement twisted boundary conditions for the deuteron and triton systems within finite volumes using the nuclear lattice EFT formalism. We investigate the finite-volume dependence of these systems with different twist angles. We demonstrate how various finite-volume information can be used to improve calculations of binding energies in such a framework. Our results suggests that with appropriate twisting of boundaries, infinite-volume binding energies can be reliably extracted from calculations using modest volume sizes with cubic length $L \approx 8$–14 fm. Of particular importance is our derivation and numerical verification of three-body analogs of "i-periodic" twist angles that eliminate the leading-order finite-volume effects to the three-body binding energy.

DOI: 10.1103/PhysRevC.93.054002

I. INTRODUCTION

Numerical simulations of nuclear observables often utilize finite volumes (FVs) to perform calculations. Lattice quantum chromodynamics (LQCD) calculations of quarks and gluons, for example, utilize cubic volumes with spatial length L typically of size $\sim$ 4–6 fm. Nuclear lattice effective field theory (NLEFT) calculations using nucleon degrees of freedom, however, employ volumes that are an order of magnitude larger. Despite being intrinsically stochastic, both methods have calculated nuclear binding energies of light hadronic systems with impressive, quantitative uncertainties. Recent LQCD calculations, albeit at unphysical pion masses, have calculated the binding energies of S-shell nuclei and light hypernuclei [1–8]. Nuclear lattice EFT calculations have readily performed binding-energy calculations of P-shell nuclei [9–13] and some medium mass nuclei [14]. With ever-increasing computer resources, calculations of such systems will become even more precise.

All of these calculations, however, suffer from a systematic error that cannot be reduced from increased computer resources: The calculated energies in a finite volume differ from their infinite-volume counterparts. In principle, this finite-volume (FV) error can be removed by performing calculations of energies in multiple volumes followed by an extrapolation to infinite volume. In practice, this is very difficult owing to the large computational costs of performing calculations in multiple volumes. However, the number of different volume calculations needed to perform a reliable extrapolation may not be exceedingly large if the functional dependence of the FV correction is known. For the two-body system with periodic boundary conditions, for example, the finite-volume correction to the binding energy is well known and the leading-order contribution scales as $\exp(-\kappa L)/L$, where κ is the binding momentum [15,16]. In Ref. [17] the functional dependence for three identical bosons in a finite volume (with periodic boundary conditions) and at the unitary limit was derived and was also determined to fall off exponentially with volume size. For higher A-body systems, the dependence is also expected to be exponential, but a general formula is yet to be determined.

Periodic boundary conditions (PBCs) are a specific case of twisted boundary conditions (TBCs) [18] at the faces of the cubic volume. These "twist" conditions can be parametrized by a vector of angles θ_i at each boundary, with range $0 \leqslant \theta_i < 2\pi$, such that

$$\psi(\mathbf{x} + \mathbf{n}L) = e^{i\boldsymbol{\theta}\cdot\mathbf{n}}\psi(\mathbf{x}). \tag{1}$$

Equation (1) shows that $\theta_i = 0$ corresponds to PBCs, while $\theta_i = \pi$ gives antiperiodic boundary conditions (aPBCs). In LQCD, TBCs are equivalent to introducing a background U(1) gauge field imposed on the quarks, subsequently endowing them with an arbitrary momentum dependent on the twist angle [19,20]. With TBCs momentum states are no longer restricted to the discrete modes within a box with PBCs, and therefore calculations with different twist boundary conditions will give rise to different finite-volume corrections. As initially found within condensed-matter calculations, averaging results with different twist angles significantly cancels finite-volume effects [21]. This has motivated the use of "twist averaging" in LQCD calculations to reduce the finite-volume dependence in hadronic masses [22] and more recently to calculations of phases of nuclear matter in dense astrophysical environments [23].

Because of the nonlinear nature of interactions in the nonperturbative regime between quarks and gluons and also between nucleons, twist averaging does not completely eliminate finite-volume effects. To what extent it does eliminate finite-volume effects is an open question and most certainly depends on the nature of interactions. In Ref. [24] the behavior of finite-volume corrections for the two-body system was investigated for specific sets of twist angles. It was found that certain linear combinations of twist angles indeed reduce significantly finite-volume effects. Just as important, it was shown that a particular set of twist angles ($\theta_i = \pi/2$), dubbed "i-periodic," also significantly reduced the leading-order exponential dependence of the finite volume.

In this paper we extend the work done in Ref. [24] to three-body systems. Except for particular three-body limits (see, e.g., Ref. [17]), analytic calculations in this regime are not possible and we utilize the NLEFT formalism to perform

our calculations. In this case, nucleons are the relevant degrees of freedom, not quarks, and therefore twist angles are applied to nucleon state functions directly. We perform a detailed statistical analysis of our calculations, accounting for and propagating all relevant systematic errors in our extrapolations. From our analysis we find the analog of i-periodic angles for the three-body system, which not only reduces finite-volume effects, but cancels exactly the leading-order FV contribution.

Our paper is organized as follows. In Sec. II we discuss the formalism for the implementation of twisted boundaries on general terms. We then derive in Sec. III the leading-order nonrelativistic finite-volume corrections (with twists), focusing on the two- and three-body systems. We describe in detail in Sec. IV the application of twists within NLEFT algorithms, which we coded specifically for this work. Included in this same section is an enumeration of sources of systematic errors owing to lattice artifacts and the finite volume and a detailed discussion of our error analysis used to propagate errors. We present results of the two-body (deuteron) system and the three-body (triton) system in Secs. V and VI, respectively. We reserve Sec. VII for a discussion of discretization effects and the potential impact they have on large twist calculations. Finally, we recapitulate our findings and discuss possible future applications in Sec. VIII.

II. IMPLEMENTATION OF TWISTED BOUNDARY CONDITIONS FOR N-BODY SYSTEMS

Assuming a nonrelativistic N-body system, this system's state can be written as a linear combination of tensor products of the individual particle states which include their internal quantum numbers,

$$|\mathcal{N}_1(I_1,S_1)\rangle \otimes \cdots \otimes |\mathcal{N}_N(I_N,S_N)\rangle,$$

where I_i and S_i refer to the isospin and spin of the ith nucleon, respectively. To realize such states computationally, an appropriate bra basis, either in configuration or momentum space, must be used. For example, momentum space calculations using a finite cube with PBCs would utilize a discrete momentum basis $\boldsymbol{p}_n = 2\pi \boldsymbol{n}/L$, where $\boldsymbol{n}$ represents a triplet of integers. With an eye towards our lattice simulations presented in later sections, we adopt a discretized coordinate basis, $\boldsymbol{r} \mapsto a\boldsymbol{n}$, where a is the lattice spacing between lattice nodes. We denote this discretized basis as $|\boldsymbol{n}\rangle$. We stress that the results of this section do not depend on the choice of basis, however.

A spatial cutoff L is introduced by limiting the basis to a cubic box of volume L^3 with the application of particular boundary conditions at the faces of the cube. This introduces finite-volume effects (errors) that can only be removed by extrapolating to infinite volume, $L \to \infty$. In this paper, we focus our analysis mainly on these finite-volume effects for the lattice. Objects defined inside the box, such as matrix elements of operators using the discretized basis $|\boldsymbol{n}\rangle$, will be denoted with a subscript L to differentiate them from their infinite-volume counterparts.

The most commonly used boundary conditions are periodic boundary conditions (PBCs), where the wave function is periodically continued outside of the box,[1] which, in turn, produces images of the wave function outside of the original cubic volume. Periodic boundary conditions are just a subset of the more general TBCs, defined as follows:

$$ {}_i\langle \boldsymbol{x}_i + L\boldsymbol{n}|\Psi_L\rangle_N = {}_i\langle \boldsymbol{x}_i|\Psi_L\rangle_N e^{i\boldsymbol{\phi}_i\cdot\boldsymbol{n}}, \quad \forall\, \boldsymbol{x}_i \in L^3, \quad \forall\, \boldsymbol{n} \in \mathbb{Z}^3. \tag{2}$$

The variable $\boldsymbol{\phi}_i \in \mathbb{R}^3$ represents the twisted boundary angle of the ith particle with components for each spatial direction. Suppressing the spin and isospin components, one can now define a basis for the discretized box (with N_L nodes in each spatial direction where $L = aN_L$), which satisfies TBCs and is useful for computing matrix elements,

$$\begin{aligned} |\mathcal{N}_{i,L}\rangle &= \sum_{\boldsymbol{n}\in\mathbb{Z}^3} \mathcal{N}_{i,L}(\boldsymbol{n})|\boldsymbol{n}\rangle_i \\ &= \frac{1}{\sqrt{M}^3} \sum_{\substack{\boldsymbol{m}\in\mathbb{Z}^3 \\ \boldsymbol{n}\in N_L^3}} \mathcal{N}_{i,L}(\boldsymbol{n}+N_L\boldsymbol{m})\cdot|\boldsymbol{n}+N_L\boldsymbol{m}\rangle_i \\ &= \frac{1}{\sqrt{M}^3} \sum_{\substack{\boldsymbol{m}\in\mathbb{Z}^3 \\ \boldsymbol{n}\in N_L^3}} \mathcal{N}_{i,L}(\boldsymbol{n}) e^{i\boldsymbol{\phi}_i\cdot\boldsymbol{m}} e^{-i\boldsymbol{\phi}_i\cdot\boldsymbol{n}/N_L} \\ &\quad \times e^{i\boldsymbol{\phi}_i\cdot\boldsymbol{n}/N_L}|\boldsymbol{n}+L\boldsymbol{m}\rangle_i \\ &=: \sum_{\boldsymbol{n}\in N_L^3} \tilde{\mathcal{N}}_{i,L}(\boldsymbol{n})|\boldsymbol{n}\rangle_i^{\boldsymbol{\phi}_i}, \end{aligned} \tag{3}$$

where we have used the following definitions:

$$M^3 := \sum_{\boldsymbol{m}\in\mathbb{Z}^3} 1, \quad \tilde{\mathcal{N}}_{i,L}(\boldsymbol{n}) := \mathcal{N}_{i,L}(\boldsymbol{n})\cdot e^{-i\boldsymbol{\phi}_i\cdot\boldsymbol{n}/N_L}.$$

All phases can be absorbed by the newly defined basis states $|\boldsymbol{n}\rangle_i^{\boldsymbol{\phi}_i}$ and the wave function $\tilde{\mathcal{N}}_{i,L}(\boldsymbol{n})$. This new "twisted basis," which we denote collectively by $\{|\boldsymbol{n}\rangle_i^{\boldsymbol{\phi}_i}\}$, can be understood as a grid of vectors multiplied by a phase associated with the different images of the original cube:

$$|\boldsymbol{n}^{\boldsymbol{\phi}_i}\rangle_i := \frac{1}{\sqrt{M}^3} \sum_{\boldsymbol{m}\in\mathbb{Z}^3} e^{i\boldsymbol{\phi}_i\cdot(\boldsymbol{n}+N_L\boldsymbol{m})/N_L}\cdot|\boldsymbol{n}+N_L\boldsymbol{m}\rangle_i. \tag{4}$$

Note that this description of twisted boundary states is, in general, different from the twisting convention used in lattice QCD. In lattice QCD one directly applies twists to the quarks and, in principle, there are different associated twist angles for each quark flavor. In our case the twists are directly applied to the configuration space coordinates of the nucleons. Thus, the number of twists is directly related to the number of nucleons; for N nucleons one could choose N different twist angles.

We note that for numerical simulations, there is some freedom in how one implements TBCs. Typically, TBCs are applied at the boundaries of the box where the application of the phase ϕ_i only occurs when a particle passes the boundary. We have instead chosen to apply twists incrementally $\propto \phi_i/N_L$

[1] This kind of behavior can also be defined for a finite continuous space.

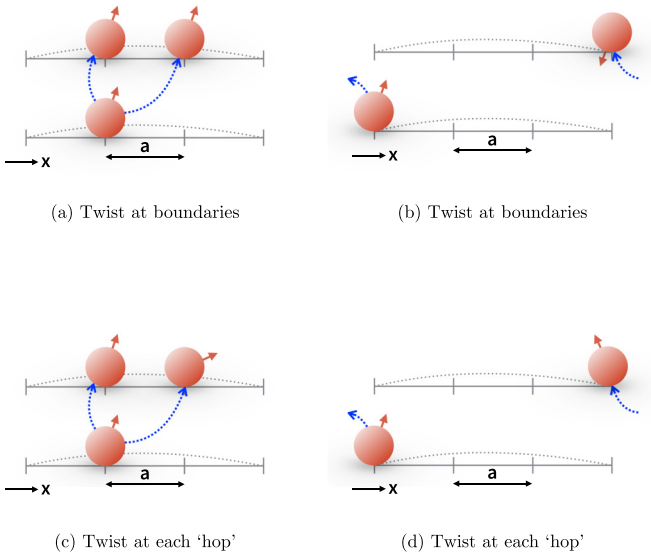

(a) Twist at boundaries (b) Twist at boundaries

(c) Twist at each 'hop' (d) Twist at each 'hop'

FIG. 1. A demonstration of the different choices of twisted boundary basis for a simple 1+1 dimensional lattice with antiperiodic boundary conditions in spatial direction ($\phi = \pi$). The phase of each particle is represented by the direction of the solid arrow.

each time a particle changes its coordinates within the volume. In this manner, the accumulation of the entire phase ϕ_i also occurs when a particle passes a boundary. In Fig. 1 we provide a schematic comparison of our twist basis to the case where twists are applied at the boundaries only. In the demonstrated case of antiperiodic boundaries, one has that the wave function flips its sign after a shift in L, $\psi(\boldsymbol{x} + \boldsymbol{e}L) = -\psi(\boldsymbol{x})$, $|\boldsymbol{e}| = 1$. Figures 1(a) and 1(b) use a basis where the boundary conditions are just applied at the edges of the spatial box. For this basis, the wave function only changes its phase when the particle "hops" outside of the box [Fig. 1(b)] but stays the same if moving within the box [Fig. 1(a)]. Figures 1(c) and 1(d) use the previously defined twisted boundary basis where a partial phase is applied each time a particle changes its spatial direction. After N_L steps in the same spatial direction, the accumulated phase becomes π and thus the wave function changes its sign. This behavior also holds true at the boundaries; however, it depends on the direction of the hops.

The main reason for including the twisted boundary phases at each particle hop is that this procedure ensures translational invariance at each point on the lattice, including the boundaries, and is thus more amenable to the NLEFT formalism. As a consequence of the translational invariance, the momentum modes in the lattice are well defined,

$$\langle \boldsymbol{p}|\boldsymbol{x}\rangle_i^{\boldsymbol{\phi}_i} = \exp\left(\frac{2\pi i}{L}\,\boldsymbol{x}\cdot\boldsymbol{n}_p\right)\delta^{(3)}(L\boldsymbol{p} - 2\pi\boldsymbol{n}_p - \boldsymbol{\phi}_i). \quad (5)$$

The δ function in Eq. (5) shows that the allowed momenta inside the box are shifted by the twists for each particle,

$$\boldsymbol{p} = \frac{2\pi\boldsymbol{n}_p + \boldsymbol{\phi}_i}{L}. \quad (6)$$

It is therefore possible to induce a nonzero center-of-mass (c.m.) energy for the zero-momentum modes, which is proportional to the twist angles,

$$E_0^{(\text{c.m.})} = \frac{\boldsymbol{P}_0^2}{2M_{\text{c.m.}}} = \frac{1}{2M_{\text{c.m.}}}\left(\sum_{i=1}^{N}\boldsymbol{\phi}_i\right)^2. \quad (7)$$

This c.m. motion must be accounted for when comparing calculations of the relative binding energies of N-body systems. We note that twist angles subject to the constraint that $\boldsymbol{\phi}_1 + \cdots \boldsymbol{\phi}_N = 0$ will induce no c.m. motion.

To conclude this section, we consider the matrix element of some arbitrary operator O using the basis in Eq. (4),

$$\langle \boldsymbol{m}_1^{\boldsymbol{\phi}_1}, \cdots; \boldsymbol{m}_N^{\boldsymbol{\phi}_N}|\,O\,|\boldsymbol{n}_1^{\boldsymbol{\phi}_1}, \cdots; \boldsymbol{n}_N^{\boldsymbol{\phi}_N}\rangle. \quad (8)$$

As the operator O can be written in terms of products over creation and annihilation operators, it suffices to consider the following term,

$$\begin{aligned}&\sum_{\boldsymbol{n}'\in\mathbb{Z}^3} a_i^\dagger(\boldsymbol{n}'+\boldsymbol{l}\,)a_i(\boldsymbol{n}')|\boldsymbol{n}^{\phi_i}\rangle_i \\ &\quad= \frac{1}{\sqrt{M}^3}\sum_{\boldsymbol{m}\in\mathbb{Z}^3} e^{i\boldsymbol{\phi}_i\cdot(\boldsymbol{n}+N_L\boldsymbol{m})/N_L}|\boldsymbol{n}+\boldsymbol{l}+N_L\boldsymbol{m}\rangle_i \\ &\quad= |(\boldsymbol{n}+\boldsymbol{l})^{\phi_i}\rangle_i e^{-i\boldsymbol{\phi}_i\cdot\boldsymbol{l}/N_L}. \end{aligned} \quad (9)$$

This term is off diagonal in the basis of creation and annihilation operators and represents a "hopping term" from site $\boldsymbol{n}$ to site $\boldsymbol{n}+\boldsymbol{l}$. Equation (9) explicitly shows how a particle picks up an incremental phase through such a translation between sites. More generally, any operator O with nonzero off-diagonal matrix elements in creation and annihilation operators will be modified by a phase within the "twisted basis,"

$$\begin{aligned}&\langle \boldsymbol{m}_1^{\boldsymbol{\phi}_1}, \cdots; \boldsymbol{m}_N^{\boldsymbol{\phi}_N}|\,O\,|\boldsymbol{n}_1^{\boldsymbol{\phi}_1}, \cdots; \boldsymbol{n}_N^{\boldsymbol{\phi}_N}\rangle \\ &\quad= \langle \boldsymbol{m}_1^{\boldsymbol{0}}, \cdots; \boldsymbol{m}_N^{\boldsymbol{0}}|\,O\,|\boldsymbol{n}_1^{\boldsymbol{0}}, \cdots; \boldsymbol{n}_N^{\boldsymbol{0}}\rangle \\ &\qquad\times \exp\left[i\sum_{i=1}^{N}\boldsymbol{\phi}_i/N_L\cdot(\boldsymbol{n}_i - \boldsymbol{m}_i)\right]. \end{aligned} \quad (10)$$

Therefore, the off-diagonal N-body matrix element with TBCs are equal to the N-body matrix element with PBCs multiplied by a phase that depends on the twist angles. It is important to stress that these matrix elements still represent a Hermitian matrix if the evaluated operator is Hermitian as well. In other words, twisted boundaries do not induce (extra) sign oscillations.

III. NONRELATIVISTIC FINITE-VOLUME EFFECTS

As already mentioned, the finite-volume corrections as a function of twist angles has been previously determined in Ref. [24] in the form of quantization conditions. If one assumes the interaction is S-wave dominated and therefore ignores the mixing angle and D-wave contributions (and higher), the finite-volume corrections can be expanded in a series of exponentials with amplitudes that depend on the twist angles. We provide the leading order (LO), next to leading order (NLO), and next to next to leading order (NNLO) terms in this expansion, with their accompanying twist-angle dependence,

TABLE I. Twist dependence of different orders for the S-wave deuteron finite-volume effects.

Order	Scaling in L	Twist dependence
LO	$\exp(-\kappa L)/L$	$2[\cos(\theta_x)+\cos(\theta_y)+\cos(\theta_z)]$
NLO	$\exp(-\sqrt{2}\kappa L)/(\sqrt{2}L)$	$4[\cos(\theta_x)\cos(\theta_y)+\cos(\theta_x)\cos(\theta_z)+\cos(\theta_y)\cos(\theta_z)]$
NNLO	$\exp(-\sqrt{3}\kappa L)/(\sqrt{3}L)$	$8\cos(\theta_x)\cos(\theta_y)\cos(\theta_z)$

in Table I. We use these functional forms to perform our fits of our deuteron twist calculations in later sections.

An analogous expansion for the general three-body system is unfortunately not known. To motivate our functional form that we use for fitting our triton results, we present a nonrelativistic derivation of finite-volume corrections. This derivation follows closely that of [25–29] and provides the leading-order finite-volume dependence of the binding energy. The exponential dependence of higher-order terms can, in principle, be determined using this method, but the exact form of the amplitude at each order is only known if the complete form of the asymptotic many-body wave function can be determined, which is not the case here. As such, these unknown amplitudes are folded into our systematic uncertainties, as described in later sections.

To arrive at our final expression of the LO finite-volume twist-dependent correction for the three-body system, we first present the derivation for the two-body case as originally shown in Ref. [29]. For nonrelativistic systems within a finite volume of spatial size L^3 with periodic boundary conditions, the physical quantities inside the box overlap with copies of themselves. As an example, the potential represented in L^3 is given by

$$V_L(\boldsymbol{r}) = \sum_{\boldsymbol{n}\in\mathbb{Z}^3} V(\boldsymbol{r}+\boldsymbol{n}L), \quad \forall\, \boldsymbol{r}\in L^3, \tag{11}$$

where V is the infinite-volume representation of the potential. Accordingly, a bound solution to the Schrödinger equation will also have a similar form of periodicity,

$$(\hat{H}_0+\hat{V}_L)|\psi_L\rangle = E_L(L)|\psi_L\rangle, \quad \langle \boldsymbol{r}+\boldsymbol{n}L|\psi_L\rangle = \langle \boldsymbol{r}|\psi_L\rangle. \tag{12}$$

As the finite-volume solution should converge against the infinite-volume solution for increasing L, one can define the finite-volume energy shift by its deviation from the infinite-volume solution,

$$\Delta E_L(L) := E_L(L) - E_\infty, \tag{13}$$

which should converge to zero for large L. When rewriting the finite-volume wave function as periodic copies of the infinite-volume wave function plus corrections

$$\begin{aligned} |\psi_L\rangle &= |\psi_0\rangle + \lambda|\epsilon\rangle, \\ \langle \boldsymbol{r}|\psi_0\rangle &:= \sum_{\boldsymbol{n}\in\mathbb{Z}^3} \langle \boldsymbol{r}+\boldsymbol{n}L|\psi_\infty\rangle, \quad \forall\, \boldsymbol{r}\in L^3, \end{aligned} \tag{14}$$

the finite-volume energy shift can be rewritten with infinite-volume quantities only,[2]

$$\Delta E_L(L) = \frac{\langle\psi_0|\eta\rangle}{\langle\psi_0|\psi_0\rangle} + \lambda^* \frac{\langle\epsilon|\eta\rangle}{\langle\psi_0|\psi_0\rangle}. \tag{15}$$

The state $|\eta\rangle$ is the result of the difference operator $\hat{H}_L - E_\infty$ acting on the state $|\psi_0\rangle$. Note that this result is completely general in terms of the number of nucleons. For the two-body case given one has

$$\begin{aligned} \langle\psi_0|\eta\rangle &= \langle\psi_0|\hat{H}_L - E_\infty|\psi_0\rangle \\ &= \int_{L^3} d^3\boldsymbol{x}_1 \int_{L^3} d^3\boldsymbol{x}_2 \psi_0^*(\boldsymbol{x}_1,\boldsymbol{x}_2) \\ &\quad \times [H_L(\boldsymbol{x}_1,\boldsymbol{x}_2) - E_\infty]\psi_0(\boldsymbol{x}_1,\boldsymbol{x}_2), \end{aligned} \tag{16}$$

where it is assumed that the Hamiltonian is local. As the next step, the infinite-volume information is implemented according to Eq. (14),

$$\begin{aligned} \langle\psi_0|\eta\rangle = \int d^3\boldsymbol{x}_1 d^3\boldsymbol{x}_2 \sum_{n_{i,j}\in\mathbb{Z}^3} & \psi_\infty^*(\boldsymbol{x}_1+n_{1,1}L,\boldsymbol{x}_2+\boldsymbol{n}_{1,2}L) \\ & \times [H_0 + V(\boldsymbol{x}_1+n_{2,1}L,\boldsymbol{x}_2+\boldsymbol{n}_{2,2}L) - E_\infty] \\ & \times \psi_\infty(\boldsymbol{x}_1+n_{3,1}L,\boldsymbol{x}_2+\boldsymbol{n}_{3,2}L). \end{aligned} \tag{17}$$

In the following, it is useful to transform to a relative Jacobi coordinate system $\boldsymbol{r} = \boldsymbol{x}_2 - \boldsymbol{x}_1$, $\boldsymbol{R} = (\boldsymbol{x}_1+\boldsymbol{x}_2)/2$. Assuming that the center-of-mass motion is zero, which will be the case in all our calculations that follow, one has

$$\begin{aligned} \langle\psi_0|\eta\rangle = \int_{L_r^3} d^3\boldsymbol{r} \sum_{n_i\in\mathbb{Z}_r^3} & \psi_\infty^*(\boldsymbol{r}+\boldsymbol{n}_1L) \\ & \times [H_0 + V(\boldsymbol{r}+\boldsymbol{n}_2L) - E_\infty]\psi_\infty(\boldsymbol{r}+\boldsymbol{n}_3L). \end{aligned} \tag{18}$$

The vectors $\boldsymbol{n}_i$ are obtained by the individual two-body coordinates, $\boldsymbol{n}_i = \boldsymbol{n}_{i,2} - \boldsymbol{n}_{i,1}$, and the subscript r denotes quantities that depend on these relative vectors. For $\boldsymbol{n}_2 = \boldsymbol{n}_3$ one has the infinite-volume Schrödinger operator acting on its infinite-volume solution, which provides the eigenvalue E_∞. Thus, only terms with unequal $\boldsymbol{n}_2, \boldsymbol{n}_3$ remain

$$\begin{aligned} \langle\psi_0|\eta\rangle = \sum_{n_1,n_2\in\mathbb{Z}} \sum_{n_3\neq n_2} \int d^3\boldsymbol{r}\, & \psi_\infty^*(\boldsymbol{r}+\boldsymbol{n}_1L) V(\boldsymbol{r}+\boldsymbol{n}_2L) \\ & \times \psi_\infty(\boldsymbol{r}+\boldsymbol{n}_3L). \end{aligned} \tag{19}$$

As $\psi_\infty(r) \propto e^{-\kappa r}/\mu r$ (and $\kappa^2 = -2\mu E_\infty$ being the binding momentum with the relative mass μ) in asymptotic regions r

[2]It still depends on the finite-volume Hamiltonian $\hat{H}_L$, which can be rewritten as copies of the infinite-volume Hamiltonian.

outside of the finite range of the potential, i.e., $V(r) \approx 0$, the leading-order contributions of Eq. (19) are given by $\boldsymbol{n}_1 = \boldsymbol{0} = \boldsymbol{n}_2$ and $\boldsymbol{n}_3$ being a unit vector (six different choices for three spacial dimensions and two directions each). Furthermore, the second term in Eq. (15) containing the state $|\epsilon\rangle$ scales as $e^{-2\kappa r}$ and thus only appears at higher orders [25]. For the deuteron one finds

$$\Delta E_L^{(\mathrm{LO})}(L) = \sum_{|\boldsymbol{n}|=1} \int d^3\boldsymbol{r}\, \psi_\infty^*(\boldsymbol{r}) V(r) \psi_\infty(\boldsymbol{r} + \boldsymbol{n}L). \quad (20)$$

The inclusion of arbitrary twisted boundary conditions is realized by including a phase[3] according to Eq. (2):

$$\langle \boldsymbol{x}_1 + \boldsymbol{n}_1 L, \boldsymbol{x}_2 + \boldsymbol{n}_2 L | \psi_\infty \rangle \mapsto \langle \boldsymbol{x}_1, \boldsymbol{x}_2 | \psi_\infty \rangle e^{-i\boldsymbol{\phi}_1 \cdot \boldsymbol{n}_1 - i\boldsymbol{\phi}_2 \cdot \boldsymbol{n}_2}. \quad (21)$$

When executing the coordinate transformation, the relevant term dotted into the relative box vector $\boldsymbol{n} = \boldsymbol{n}_2 - \boldsymbol{n}_1$ is now given by $\boldsymbol{\theta} = (\boldsymbol{\phi}_2 - \boldsymbol{\phi}_1)/2$ and thus the relative wave function transforms as

$$\langle \boldsymbol{r} + \boldsymbol{n}L | \psi_\infty \rangle \mapsto \langle \boldsymbol{r} | \psi_\infty \rangle e^{-i\boldsymbol{\theta} \cdot \boldsymbol{n}}. \quad (22)$$

Thus, to obtain the leading-order finite-volume energy shift for general twisted boundary conditions, the previous result for periodic boundary conditions simply gets multiplied by this phase,

$$\Delta E_L^{(\mathrm{LO})}(L, \boldsymbol{\theta}) = \sum_{|\boldsymbol{n}|=1} \int d^3\boldsymbol{r}\, \psi_\infty^*(\boldsymbol{r}) V(r) \psi_\infty(\boldsymbol{r} + \boldsymbol{n}L) e^{-i\boldsymbol{\theta} \cdot \boldsymbol{n}}. \quad (23)$$

The expression above only depends on the relative twist angle θ because we choose twist angles that ensure zero c.m. motion; i.e., $\boldsymbol{\phi}_1 + \boldsymbol{\phi}_2 = 0$.

The exponential dependence of the finite-volume corrections shown in Table I can be reproduced from this derivation, which, in turn, comes from the asymptotic behavior of the infinite-volume wave function. For example, in the case of the S wave, one finds [29]

$$\begin{aligned} \Delta E_L^{(\mathrm{LO})}(L, \boldsymbol{\theta}) &= -\frac{\sqrt{\pi} A_\kappa}{\mu} \sum_{|\boldsymbol{n}|=1} \psi_\infty^*(\boldsymbol{n}L) e^{-i\boldsymbol{\theta} \cdot \boldsymbol{n}} \\ &= -|A_\kappa|^2 \frac{e^{-\kappa L}}{\mu L} \sum_{j=1}^{3} \cos(\boldsymbol{\theta} \cdot \boldsymbol{e}_j), \end{aligned} \quad (24)$$

where $\boldsymbol{e}_j$ is the unit vector in the jth direction. Furthermore, A_κ is the amplitude of the wave function which depends on properties of the interaction, such as the the scattering length or the binding momentum $\kappa = \sqrt{-2\mu E_\infty}$.

Next-to-leading-order (NLO) terms can be obtained by systematically allowing the displacement vector $\boldsymbol{n}$ to be larger; e.g., the NLO corresponds to $|\boldsymbol{n}| = \sqrt{2}$ and so on. Though the box size scaling as well as the twist dependence of the finite-volume corrections can be computed using this method, to obtain the size of the amplitudes A_κ of the exponential decay for finite-volume energy shifts, the exact form of the asymptotic wave function needs to be known, which, in turn, depends on the specific form of the interaction.

We now turn to the three-body system. Here the only difference is that the full potential now contains three pair interactions (neglecting the three-body interaction which, when included, gives rise to the same finite-volume dependence). Thus, the state $|\eta\rangle$ now produces the leading-order term [17]

$$\Delta E_L^{(\mathrm{LO})}(L, \{\boldsymbol{\phi}_i = \boldsymbol{0}\}) = \sum_{i=1}^{3} \sum_{(\boldsymbol{n}_i, \boldsymbol{n}_j, \boldsymbol{n}_k) \in M_i} v(\boldsymbol{n}_i, \boldsymbol{n}_j, \boldsymbol{n}_k), \quad (25)$$

where $v(\boldsymbol{n}_i, \boldsymbol{n}_j, \boldsymbol{n}_k)$ is the three-body analog of Eq. (19),

$$\begin{aligned} &v(\boldsymbol{n}_i, \boldsymbol{n}_j, \boldsymbol{n}_k) \\ &:= \int d^3\boldsymbol{x}_i \int d^3\boldsymbol{y}_i\, \psi_\infty^*(\boldsymbol{x}_i, \boldsymbol{y}_i) V_i(x_i) \\ &\quad \times \psi_\infty\left(\boldsymbol{x}_i - (\boldsymbol{n}_j + \boldsymbol{n}_k)L, \boldsymbol{y}_i + \frac{1}{\sqrt{3}} (\boldsymbol{n}_j + \boldsymbol{n}_k - 2\boldsymbol{n}_i) L \right). \end{aligned} \quad (26)$$

Here $\boldsymbol{x}_i = r_j - r_k$ and $\boldsymbol{x}_2 = (r_j + r_k - 2r_i)/\sqrt{3}$ are a particular choice of Jacobi coordinates, which describe the three-body system. The set M_i is chosen such that Eq. (25) reassembles the leading-order difference of the finite-volume Hamiltonian and the infinite-volume energy; e.g., the vectors are chosen such that the hyperradius $\rho^2 = \sum_i (\boldsymbol{r}_i + \boldsymbol{n}_i L)^2$ is minimal while $\boldsymbol{n}_j \neq \boldsymbol{n}_k$,

$$\begin{aligned} M_i := \min\nolimits_\rho (\{(\boldsymbol{n}_i, \boldsymbol{n}_j, \boldsymbol{n}_k) \in \mathbb{Z}^9 | \{i,j,k\} = \{1,2,3\} \\ \text{and} \quad \boldsymbol{n}_j - \boldsymbol{n}_k \neq 0\}). \end{aligned} \quad (27)$$

Similar to the two-body case, an extension of this result to twisted boundaries is given by multiplying this expression with a phase containing a sum over all twist angles,

$$\Delta E_L^{(\mathrm{LO})}(\{\boldsymbol{\phi}_i\}) = \sum_{i=1}^{3} \sum_{(\boldsymbol{n}_i, \boldsymbol{n}_j, \boldsymbol{n}_k) \in M_i} v(\boldsymbol{n}_i, \boldsymbol{n}_j, \boldsymbol{n}_k)\, e^{-i \sum_{l=1}^{3} \boldsymbol{\phi}_l \cdot \boldsymbol{n}_l}, \quad (28)$$

where in this case we express the twist angles in the single-particle basis. Equation (28) gives the LO twist-dependent finite-volume dependence of the three-body system. As we numerically verify later, appropriate choices of twist angles can eliminate this LO dependence.

IV. APPLYING TWISTS WITHIN THE NLEFT FORMALISM

To study the effects of the finite volume on two- and three-body systems, we perform calculations on a discretized space-time lattice within a cubic volume. Our implementation follows closely that of the NLEFT formalism. Though the NLEFT algorithm is well documented (for a review of NLEFT, see Ref. [30]), we provide a cursory description of our

[3]Note the relative minus sign of the phase. This sign for the infinite-volume wave-function phase ensures that the wave function on the lattice transforms as in Eq. (2).

algorithm mainly to point out differences with past NLEFT calculations and to describe our implementation of TBCs within the NLEFT formalism.

A. Twists on the transfer matrix $\mathcal{M}$

To obtain results of nuclear observables on a lattice, one computes the trace of products of the transfer matrix, $\mathcal{M}$, which in our case is identified with the chiral interaction of nucleons. Formally, the transfer matrix in Euclidean time is given by the normal-ordered exponential of the corresponding effective Hamiltonian,

$$\mathcal{M} := : \exp(-H a_t) : . \tag{29}$$

The spectrum of H can be ascertained from eigenvalues of the transfer matrix $\mathcal{M}$,

$$\mathcal{M}|\psi_n\rangle = \epsilon_n|\psi_n\rangle, \quad \epsilon_0 > \epsilon_i, \quad \forall\, i > 0. \tag{30}$$

In particular, the ground-state energy E_0 of the system is related to the largest eigenvalue of $\mathcal{M}$, which we denote as ϵ_0, and can be obtained through the following logarithmic derivative

$$E_0 = -\frac{\ln(\epsilon_0)}{a_t}. \tag{31}$$

The Lagrangian that generates the transfer matrix contains the leading-order chiral contact interactions given in, for example, Ref. [31]. Effectively one obtains a two-body force as well as the one-pion exchange at leading order,

$$V_\chi^{(\mathrm{LO})}(q) = V_{NN}^{(\mathrm{LO})}(q) + V_{\pi N}^{(\mathrm{LO})}(q), \tag{32}$$

where

$$V_{\pi N}^{(\mathrm{LO})}(q) = -\left(\frac{g_A}{2f_\pi}\right)^2 \frac{(\boldsymbol{\sigma}_1\cdot\boldsymbol{q})(\boldsymbol{\sigma}_2\cdot\boldsymbol{q})}{q^2+m_\pi^2}\,(\tau_1\cdot\tau_2). \tag{33}$$

Here the nucleon mass and the pion mass are set; their physical values are $m_N = 938.92$ MeV and $m_\pi = 134.98$ MeV. The pion decay constant is $f_\pi = 92.2$ MeV and the axial coupling has a strength of $g_A = 1.29$ respecting the Goldberger-Treiman discrepancy for representing the strong πNN coupling. Furthermore, the momentum $\boldsymbol{q} = \boldsymbol{p}' - \boldsymbol{p}$ is the nucleon momentum transfer. In this work, the contact potential was implemented using a Gaussian-like smearing in momentum space similar to the one used in Ref. [32],

$$\begin{aligned} V_{NN}^{(\mathrm{LO})}(q) = (&c_{\mathrm{SU4}} + c_{\mathrm{I}}\,\tau_1\tau_2 + c_{\mathrm{S}}\,\boldsymbol{\sigma}_1\cdot\boldsymbol{\sigma}_2 \\ &+ c_{\mathrm{SI}}\,\tau_1\tau_2\,\boldsymbol{\sigma}_1\cdot\boldsymbol{\sigma}_2)e^{-b_4 q^4}. \end{aligned} \tag{34}$$

Furthermore, the low energy coefficients (LECs) (c_{SU4},c_{S}, c_{I},c_{SI}) were related to each other through the leading-order singlet and triplet coefficients C_S and C_T when evaluating nucleonic matrix elements,

$$\begin{aligned} c_{\mathrm{SU4}} &= \tfrac{1}{16}(3c_{\mathrm{S}} + 3c_{\mathrm{T}}), \quad c_{\mathrm{S}} = \tfrac{1}{16}(-3c_{\mathrm{S}} + c_{\mathrm{T}}), \\ c_{\mathrm{I}} &= \tfrac{1}{16}(3c_{\mathrm{S}} - c_{\mathrm{T}}), \quad c_{\mathrm{SI}} = \tfrac{1}{16}(-c_{\mathrm{S}} - c_{\mathrm{T}}). \end{aligned} \tag{35}$$

The contact interactions were fitted to reproduce the deuteron binding energy as well as the ${}^3S_1$ scattering length. We tabulate their values, as well as other parameters relevant to our simulations, in Table II. To reduce the dimensionality of the problem, the spin-breaking part of the pion exchange was assumed to be small and computations with this part were done for one specified spin channel only. This induced a small error when comparing to the "experimental result" at the order of 0.05 MeV for the deuteron.

TABLE II. Numerical values of parameters used in our simulations.

$1/a_L$ (MeV)	$1/a_T$ (MeV)	c_S (10^{-5} MeV^{-2})	c_T (10^{-5} MeV^{-2})	$\Delta^{(n)}$ $\mathcal{O}(a^{2\times n})$	b_4 (MeV^4)
100	150	−4.2000	−6.0513	$\mathcal{O}(a^{2\times 4})$	0.07

Because of our "low-order" interaction, we do not expect to have perfect agreement for the three-body energy levels when compared to experiment. However, because the goal of this paper is to emphasize the dependence of the binding energy of few-body systems on FV corrections, this level of simplicity for the nucleon interactions is sufficient. As such, one should compare calculated energy levels in a fixed volume to their converged results for large (infinite) volumes instead of to the experimental results themselves.

Furthermore, at this order our potential does not contain any derivatives acting on the nucleon coordinates and therefore does not induce translations on the nucleon states. The inclusion of TBCs is therefore realized by implementing Eq. (10) for the kinetic Hamiltonian operators only.

As a final comment, we point out that the normal ordering of the transfer matrix for two nucleons $\mathcal{M}^{(2)}$ is exact at order a_t^2,

$$\mathcal{M}^{(2)} = \mathbb{1} - a_t\big(H_0^{(1)} + H_0^{(2)} + V^{(1,2)}\big) + a_t^2 H_0^{(1)} H_0^{(2)}. \tag{36}$$

To identify the c.m. motion of such a system, one can rewrite the absolute momenta of the individual particles as combinations of the c.m. momentum $\boldsymbol{P}$ and the relative momentum $\boldsymbol{q}$,

$$\begin{aligned} \mathcal{M}^{(2)} = \mathbb{1} &- a_t\big(H_0^{(\mathrm{rel})} + H_0^{(\mathrm{c.m.})} + V^{(\mathrm{rel})}\big) \\ &+ a_t^2\left[\frac{1}{4}\big(H_0^{(\mathrm{rel})} + H_0^{(\mathrm{c.m.})}\big)^2 - \left(\frac{\boldsymbol{P}\cdot\boldsymbol{q}}{M_{\mathrm{c.m.}}}\right)^2\right]. \end{aligned} \tag{37}$$

Equation (37) shows that the term of second order in a_t couples c.m. motion to relative motion for nonzero c.m. momenta. Thus, the procedure of subtracting the c.m. motion from the computed spectrum is more complicated. If one computes the spectrum of a two-nucleon system using general twisted boundaries, the energy eigenvalues of the transfer matrix are shifted by the nonzero c.m. contributions generated by these twists. This also holds true for more general N-body systems as well. For this current work we avoid the extra complication of nonzero c.m. coupling by utilizing twists that induce zero c.m. motion, which is determined by the following constraint:

$$\sum_{n=1}^{N} \boldsymbol{\phi}_n = 0. \tag{38}$$

B. Identification of systematic errors and description of error analysis

Nuclear lattice EFT calculations employ Monte Carlo methods to estimate the ground-state energy of N-body systems. Because such methods are intrinsically stochastic, the extracted energies have an associated statistical uncertainty. In our case, because the dimensions of our systems are so small, we can extract our energies via direct diagonalization of the transfer matrix. Our energies therefore have no statistical uncertainty.

Nevertheless, our results are not completely free of "errors," as there still exist sources of theoretical and systematic uncertainties which can induce an effect on the final result. We enumerate these sources here and discuss each in turn below:

(i) finite-volume effects;
(ii) discretization errors;
(iii) numerical/rounding errors;
(iv) uncertainties associated with the fitting of lattice parameters (LECs on the lattice for NLEFT).

Because the aim of our study is the analysis of the FV dependence of the ground-state binding energy, the uncertainties associated with the fitting procedure of LECs are neglected. We also neglect the errors associated with discretization, which are connected to the implementation of the derivatives and the fitting of the LECs. In LQCD, when one wants to rigorously compute physical observables, one also has to take the $a \to 0$ continuum limit. Here a careful accounting of the discretization errors is needed to perform a robust extrapolation. In NLEFT this procedure is more complicated because the interactions themselves are cutoff dependent for a given order in the effective expansion. In our case we do not perform a continuum analysis because, again, we only focus on comparing the computed energies in a finite volume to their infinite-volume counterparts. As such, all our calculations use the same lattice spacing. However, even though we do not include any systematics owing to finite lattice spacing in our error propagation, we do observe discretization errors, particularly for large twist angles. We defer this point to Sec. VII where we discuss these observations in detail.

Our numerical errors are associated with the solving procedure only, which involves a Lanczos-like iteration for diagonalizing the transfer matrix and obtaining eigenvalues. This method of solving does not introduce any statistical errors. These numerical errors are of the order $\epsilon = e^{-Ea_t} \leqslant 10^{-5}$, which corresponds to an energy error budget of[4]

$$\delta E_\epsilon \leqslant \frac{\delta\epsilon}{a_T \epsilon} \simeq 0.002 \text{ MeV}. \tag{39}$$

In contrast to the previous errors, which are volume independent, we note that the FV energy corrections are only asymptotically diminishing if the potential vanishes within the cubic volume. Formally, the FV needs to be of size $L/2 \gtrsim R$, where $V(R) \simeq 0$. Furthermore, for small boxes, next-to-leading-order (NLO) FV corrections become more relevant. As an example, the functional form of the leading-order FV expression of the energy shift for two-body states does not perfectly describe our numerical results, particularly at small volumes, because the complete energy shift includes higher-order corrections described by several exponential functions of different exponents and amplitudes (see Table I for the deuteron case). Because one of our objectives of this study is to use calculations within small volumes to extract infinite-volume observables, we must explicitly take into account the errors from neglecting NLO (and higher) FV effects. We do this by estimating the size of the NLO FV systematic error, $\Delta E_L^{(\mathrm{NLO})}(L)$, and inflating our binding-energy uncertainties by this amount when performing our fitting and error analysis,

$$\Delta E_L^{(\mathrm{NLO})}(L,\phi) \mapsto \delta\big(\Delta E_L^{(\mathrm{LO})}(L,\phi)\big). \tag{40}$$

We stress that ΔE_L denotes the analytic form of the finite-volume corrections, while quantities labeled with a δ are treated as uncertainties of the computation and fitting procedure.

In principle, this NLO FV term should be interpreted as a weight for the fitting procedure, which increases the relevance of data points at larger box sizes (where NLO FV effects become less important).

With the sources of errors described above, we parametrize the total *uncertainty* for the binding energy, $\delta(E_L - E_\infty)$, by the following terms:

$$\begin{aligned}\delta(E_L - E_\infty) &\simeq \delta\big(\Delta E_L^{(\mathrm{LO})}(L,\phi)\big) + \delta E_\epsilon \\ &=: \delta E_L(L,\phi) + \delta E_\epsilon.\end{aligned} \tag{41}$$

Note that one can assume that the errors associated with this effect might be correlated, e.g., that each data point for a given twist is shifted in the same direction by the NLO FV corrections. To emphasize this, in the case of the deuteron, the known twist dependence of the NLO effects have also been computed.

Our final objective is to extract the infinite-volume binding energy E_∞, as well as the coefficients obtained by fitting the leading-order FV behavior $\Delta E_L^{(\mathrm{LO})}(L,\phi)$. To estimate the uncertainties of the fitted parameters, we employed a bootstraplike procedure in our fitting process. We first performed calculations of binding energies at different values of L and twist angles ϕ (for the total set of computations see Table III). We designate the collection of such results as D_0. From D_0 we generated N_s new distributions D_i by sampling data points within D_0 assuming the data points were randomly

TABLE III. Parameters for the computation: number of twist-angle combination, maximal box size, number of sampled distributions for the error analysis, and the lattice spatial spacing.

System	N_Φ	$N_{L,\max}$	N_s	a/fm
Deuteron	41	20	1000	1.97
Triton	121	7	1000	1.97

[4]For convenience in presentation, we always denote finite-volume effects using the symbol Δ, while errors and uncertainties used for the error estimation and propagation are labeled with the symbol δ.

distributed[5] within the interval $\delta E(L)$. Finally, the spread in our fits of the new distributions D_i provided the variations in our fit parameters. Thus, the error as well as the mean value of the fitting parameters F were obtained by sampling the new distributions $P(F)$ of fitted parameters (which contain N_s data points),

$$\mu_F = \int dF\, F\, P(F),$$
$$\Delta F^{(\pm\alpha)} \leftrightarrow \int_{\mu_F}^{\mu_F \pm \Delta F^{(\pm\alpha)}} dF\, P(F) = \pm\alpha. \tag{42}$$

In our analysis, $\alpha = 0.341$ was chosen to give 1σ confidence intervals. The overall χ^2 per degrees of freedom χ^2_{avg} is given by an average over all individual fit χ^2 for each fit of distributions D_i,

$$\chi^2_{\text{avg}} := \frac{1}{N_s} \sum_{i=1}^{N_s} \chi^2_{\text{d.o.f.}}(D_i). \tag{43}$$

V. TWO-BODY SYSTEM: THE DEUTERON

As shown in Sec. III it is possible to analytically compute the FV corrections of the binding energy for a two-body system. In general, this correction depends on the associated boundary angles $\boldsymbol{\theta}$ in relative coordinates, the box size L, as well as infinite-volume quantities,

$$E_L - E_\infty \simeq \Delta E_L^{(\text{LO})}(L,\boldsymbol{\theta}) = -\mathcal{N}^{(\text{LO})} \frac{e^{-\kappa L}}{\kappa L} \sum_{i=1}^{3} \cos(\theta_i). \tag{44}$$

Here κ is the binding momentum $\kappa^2 = -m_N E_\infty > 0$ and $\mathcal{N}^{(\text{LO})}$ is a numerical amplitude which, in general, depends on the binding energy and the nucleon mass as well as the angular-momentum quantum numbers. The boundary angle $\boldsymbol{\theta}$ is defined for the relative system and can be associated with the shift of the relative momentum. Thus, the individual nucleon twists $\boldsymbol{\phi}_i$ can be related to $\boldsymbol{\theta}$ by

$$\boldsymbol{\theta} = \frac{\boldsymbol{\phi}_2 - \boldsymbol{\phi}_1}{2}.$$

The next-to-leading-order finite-volume effects are parametrized as follows

$$\Delta E_L^{(\text{NLO})}(L) = \frac{e^{-\kappa L}}{\kappa L}\left[A_1^{(\text{NLO})}(\theta)\, e^{-(\sqrt{2}-1)\kappa L} + A_2^{(\text{NLO})}(\theta)\, \frac{1}{\kappa L}\right]. \tag{45}$$

Because the deuteron is mostly S wave, the factor containing higher partial-wave contributions is set to zero, $A_2^{(\text{NLO})}(\theta) = 0$. Because the main goal of the paper is to analyze the three-body FV effects, where this dependence is not as trivial as in the deuteron case (and analytic forms are not in general known), we initially choose twist-independent NLO errors. Such a choice is conservative and one in which we apply to the triton case as well. Furthermore, for error estimation, the error amplitude $A_1^{(\text{NLO})}(\theta)$ is assumed to be of the order of the fitted amplitudes $\mathcal{N}^{(\text{LO})}$, and we therefore set $A_1^{(\text{NLO})}(0) = \mathcal{N}^{(\text{LO})}$. We also choose twists that are antiparallel to ensure zero c.m. motion. Last, each spatial direction is boosted equally by $\phi_2 = \phi = -\phi_1$, resulting in $\boldsymbol{\theta} = \boldsymbol{\phi}$. Therefore, the finite-volume energy correction amplitude is proportional to a single cosine factor depending on the twist angle ϕ,

$$\Delta E_L^{(\text{LO})}(L,\phi) = -3\,\mathcal{N}^{(\text{LO})} \frac{e^{-\kappa L}}{\kappa L} \cos(\phi) =: A^{(\text{LO})}(\phi) \frac{e^{-\kappa L}}{\kappa L}. \tag{46}$$

We have performed calculations using 41 different twist boundary conditions, each at multiple volumes $L = aN_L$, with L from 6 fm to 40 fm and a spatial lattice spacing $a = 1.97$ fm. In Fig. 2 we show a small subset of our twist calculations with their corresponding fits. The infinite-volume binding energy of the deuteron E_∞ as well as the coefficients in front of the exponential $A^{(\text{LO})}(\phi)$, shown in Fig. 3, have been extracted from the computed data points using both a constrained fitting procedure where we enforce the same infinite volume E_∞ but different amplitude coefficient for all distributions and individual fitting procedures where we make no constraint on E_∞. The cumulative average of $N_s = 1000$ distributions within the data errors results in $\chi^2_{\text{avg}} = 0.36$. The normalized amplitudes $\mathcal{A}(\phi) := A^{(\text{LO})}(\phi)/A^{(\text{LO})}_{\text{max}} = -\cos(\phi)$ with $A^{(\text{LO})}_{\text{max}} = \max(|A(\phi)^{(\text{LO})}|)$ have been fitted to $f(\phi) = c_1\,\mathcal{A}(\phi) + c_2$ (Fig. 3).

To emphasize the convergence of the twist averaging, we show in Fig. 4 the relative deviation of the extracted binding energies and the infinite-volume binding energy using various fit ranges (from $L_{\text{start}} \approx 8$ fm to $L_{\text{end}} = L$) for periodic boundary fits, periodic and antiperiodic constrained fits, and fits with i-periodic twists. In Fig. 4, one can see results obtained without making use of the fitting error propagation, results that would have been obtained without making explicit use of the NLO FV corrections. We find that aPBC + PBC average results improve and particularly iPBC greatly improve the precision of finite-volume results compared to PBC results. These findings are in complete agreement with those of Ref. [24] and gives us confidence that our implementation of twists is correctly done. Because the computational costs grows exponentially with the size of the box, studies computing ground-state binding energies can greatly profit using such twists, particularly if similar conditions hold for more complicated N-body systems.

Examination of Fig. 3 shows that, for the two-body case with zero induced c.m. twists, the iPBCs are superior to an average over several twists. We make note of an apparent offset in our calculations, particularly around $\phi = \pi$, which can be seen by comparing the data points to the analytic dotted line in Fig. 3. Indeed, an integration over all twists points in Fig. 3 results in an offset at the order $\delta E_\infty = -0.04 \times \delta\Delta E_L^{(\text{LO})}(L,0)$. This offset leads to a larger uncertainty in our extracted energies, compared with iPBCs, even when

[5]Quantitatively similar results have been obtained for a Gaussian distribution and a uniform distribution. The propagated errors of the uniform distribution have slightly more spread.

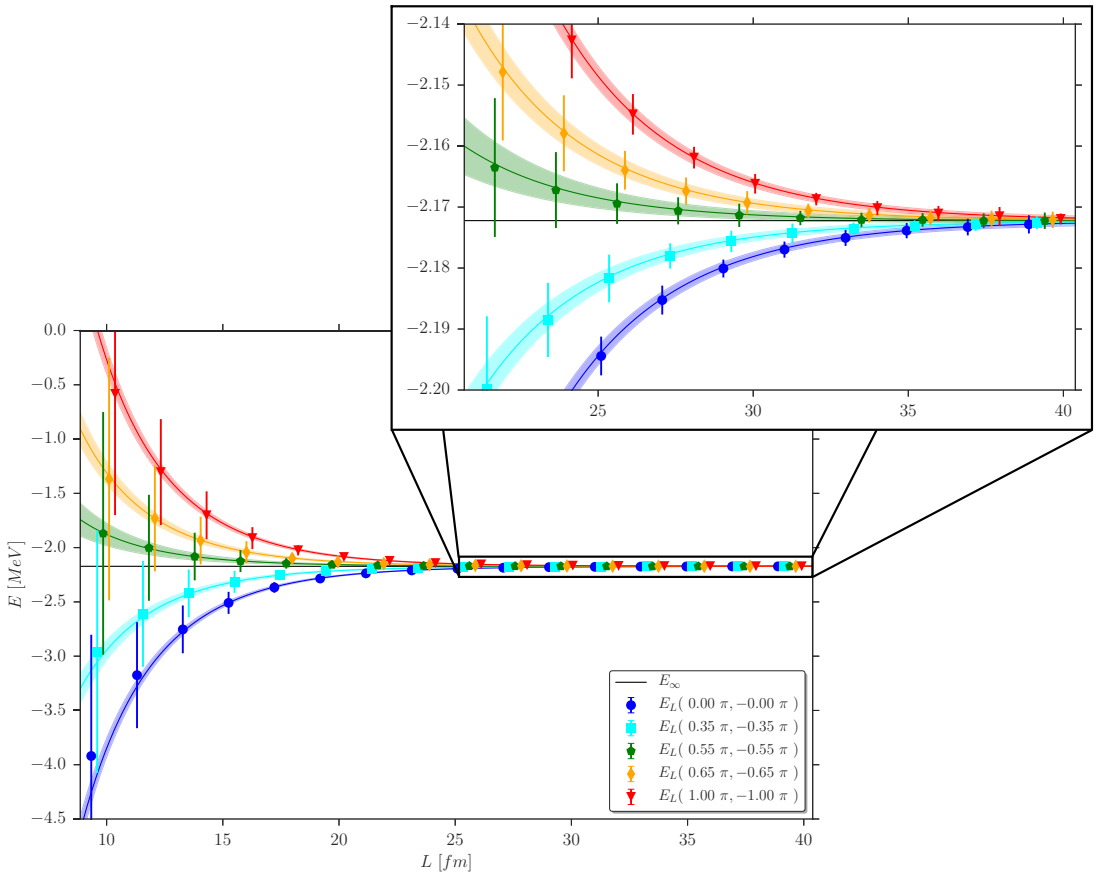

FIG. 2. Selected individual fits of two-body binding energy depending on finite volume for $L = aN_L$ with L from ≈ 8 to 40 fm and $a = 1.97$ fm. $E_B = (-2.172^{+0.000}_{-0.001})$ MeV and $\chi^2_{\text{avg}} = 0.36$ have been similar for each twist configuration according to error propagation. The error bars and error bands correspond to 1σ. Data points and bands are slightly shifted in the L direction for visualization purposes.

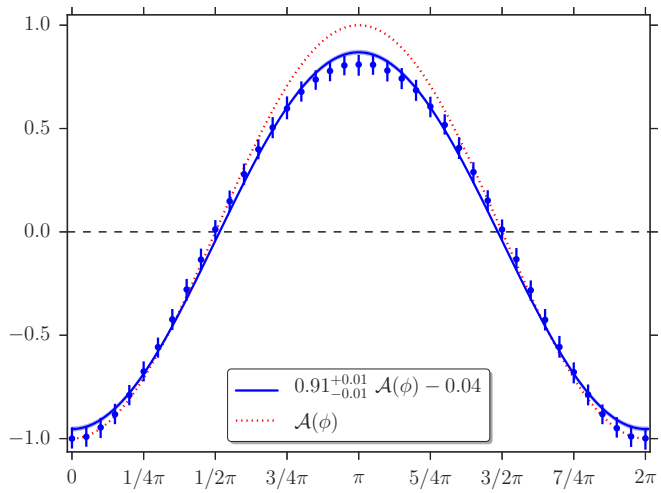

FIG. 3. Fit of two-body coefficient $\mathcal{A}(\phi)$ depending on relative twist angle $(\phi_1, \phi_2) = (\phi, -\phi)$, with $\chi^2_{\text{avg}} = 0.92$. The solid line corresponds to a fit of the form $f(\phi) = c_1\ \mathcal{A}(\phi) + c_2$, while the dotted line is the theoretical prediction $\mathcal{A}(\phi) = -\cos(\phi)$. The error bars and error bands correspond to 1σ.

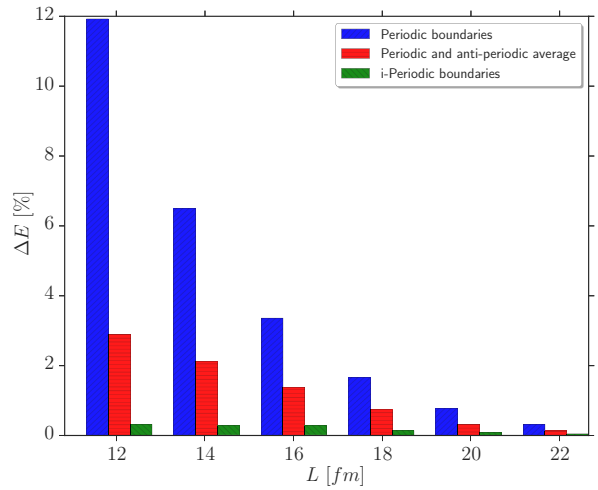

FIG. 4. Relative error of the extracted binding energy compared to the infinite-volume result as a function of maximum fit range L. The bars display the results for periodic boundaries only (left), the average of periodic and antiperiodic boundaries (middle), and i-periodic boundaries (right). This fit ignores the NLO finite-volume errors.

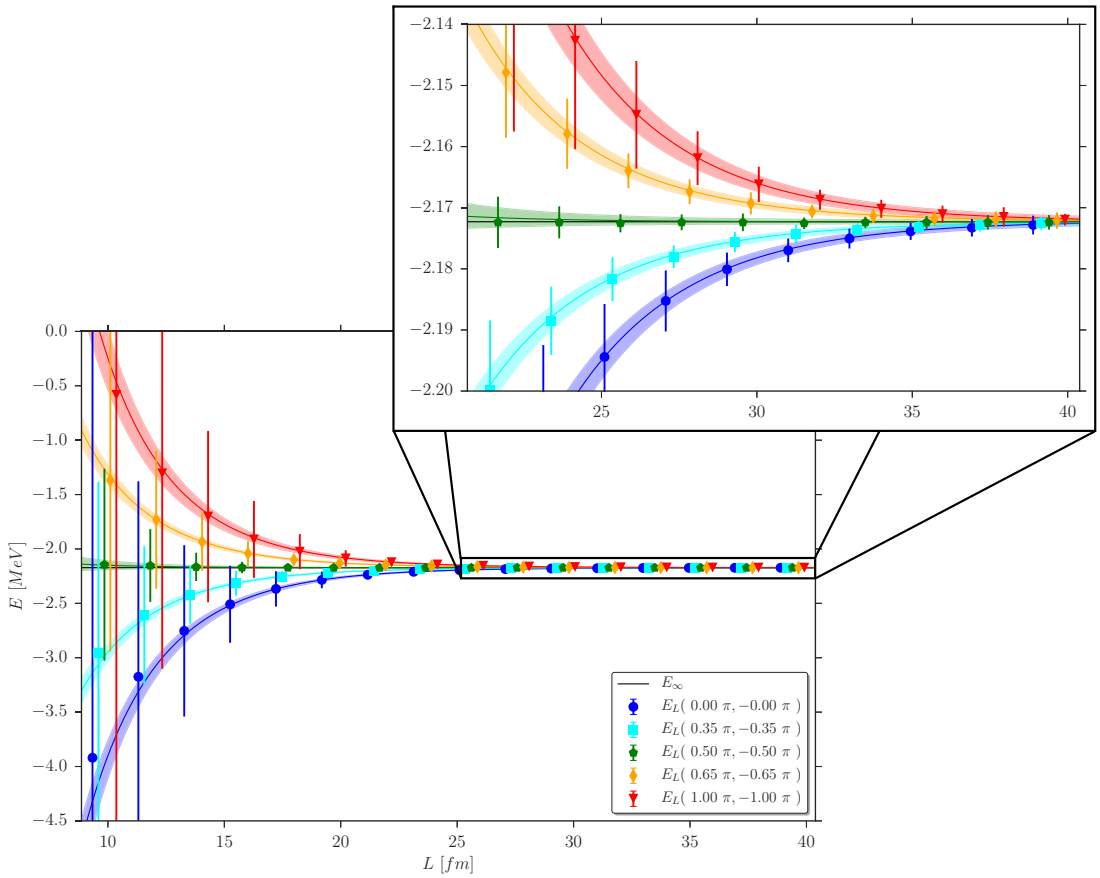

FIG. 5. Example fits for a fit range from $L \approx 8$ to 40 fm with $\chi^2_{\text{avg}} = 0.33$. Fit errors include twist-dependent NLO FV correction information. The error bars correspond to 1σ.

averaging over small sets of twists, as shown in Fig. 4. As we show in the next section, similar offsets are also seen in our three-body calculations. We return to the subject of this offset in Sec. VII.

Because the NLO finite-volume twist dependence for the deuteron is analytically known, we have also performed fits using this dependence for several fitting ranges. This analysis is based on the error propagation explained in Sec. IV B, where the NLO twist dependence and scaling of the FV effects are extracted from Table I. Again the deuteron is assumed to be purely S wave and in this case the N2LO is assumed to be twist independent. We provide the fit results in Fig. 5 and the corresponding fitting errors in Fig. 6. We find that the obtained data interval is consistent with the infinite-volume result for each fitting range (though the errors especially for small ranges are particularly large). Nevertheless, the size of the uncertainties for an aPBC plus PBC average are just slightly smaller than the uncertainties for just PBCs. This is the case because for both twists the error amplitudes $A_1^{\text{NLO}}(\phi)$ are maximal in ϕ. For the combined fit one nevertheless has relatively more data points than parameters and thus the total error of the fitted parameters reduced. For the iPBCs, however, the NLO errors are completely removed and thus accuracy is better compared to the previous twists.

Although our individual fits of E_∞ at different volumes are consistent within uncertainties, as shown in Fig. 6, we find that each of our χ^2_{avg} per degree of freedom is typically below 1 ($\chi^2_{\text{avg}} \approx 1/3$). As expected, this indicates that our results are correlated and/or our errors have been overestimated. Indeed, one source of overestimation comes from the fact that we have conservatively assigned the magnitudes of the error to be roughly of the same size as the fitted amplitude: $A_1^{(\text{NLO})}(0) \approx \mathcal{N}^{(\text{LO})}$. Nevertheless, these results allow a quantitative comparison because the overestimation is multiplicative and thus the relative size of the errors stay the same. For $L > 30$ fm, as a result of the analysis, the finite-volume errors are of the size of the numerical precision and therefore twist independent.

VI. THREE-BODY CASE: THE TRITON

The exact form of finite-volume corrections for the general three-body case has not been determined to date. In Ref. [17], however, the three-body leading-order FV corrections for three identical particles with PBCs ($\boldsymbol{\phi}_i = 0$ for $i = 1,2,3$) in the unitary limit was derived,

$$\Delta E_L^{(\text{LO})}(L, \{\boldsymbol{\phi}_i = \mathbf{0}\}) = \mathcal{N}_{\text{PB}}^{(\text{LO})} \frac{\exp\left(-\frac{2}{\sqrt{3}}\kappa L\right)}{(\kappa L)^{3/2}}. \tag{47}$$

Though this form is not rigorously applicable for our system (our system is not at the unitary limit), it is sufficient for

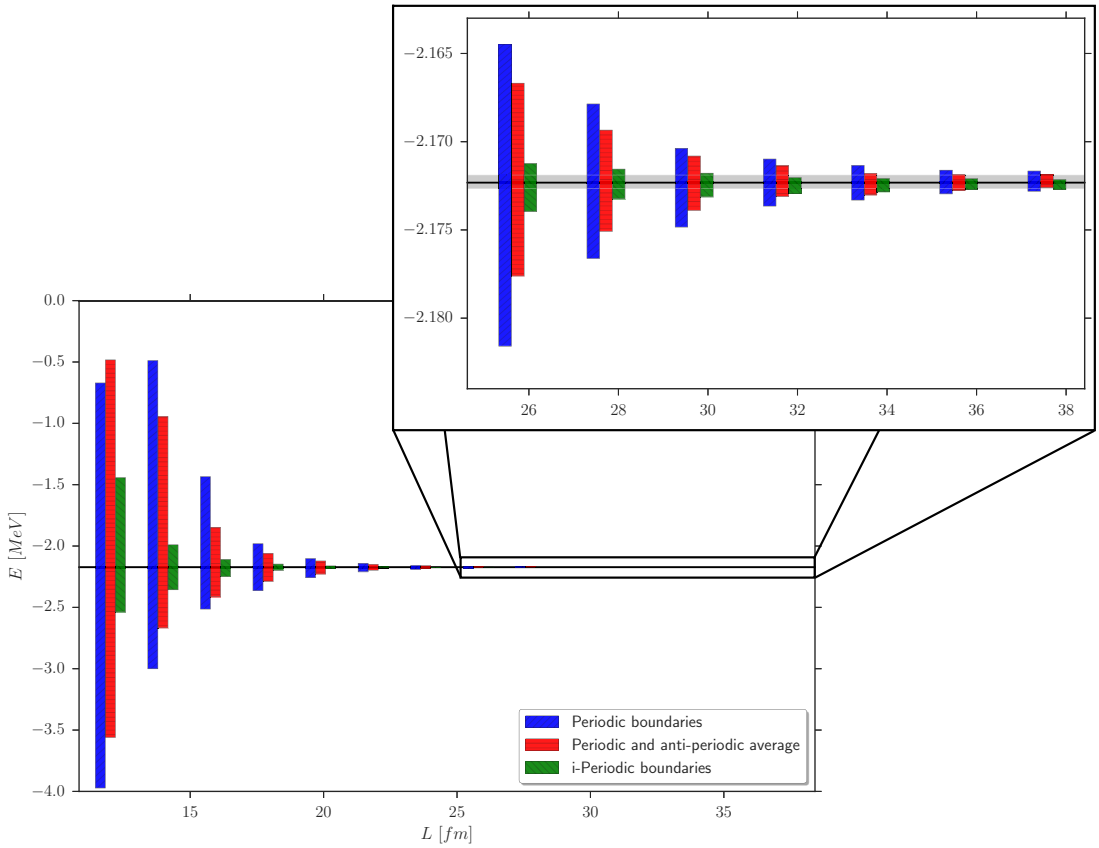

FIG. 6. Fit range dependence of deuteron binding energy. Fit errors include twist-dependent NLO FV correction information. The bars display the results for periodic boundaries only (left), the average of periodic and antiperiodic boundaries (middle), and i-periodic boundaries (right). For each individual fit, the χ^2_{avg} has been around $\chi^2_{\text{avg}} = 0.33 \pm 0.01$. The error bars correspond to 1σ.

the analysis we describe below. We stress that our main conclusions of this section do not depend on the specific FV functional dependence shown in Eq. (47).

As done in the two-body case, we assume that the NLO FV corrections come from additional powers of $(\kappa L)^{-1}$ for different partial-wave channels, as well as suppressed terms coming from the overlap of diagonally shifted images of the wave functions[6] with the original wave function,

$$\Delta E_L^{(\text{NLO})}(L,\{\boldsymbol{\phi}_i = \mathbf{0}\}) = \mathcal{N}_{1,\text{PB}}^{(\text{NLO})} \frac{\exp\left(-\sqrt{\frac{8}{3}}\kappa L\right)}{(\kappa L)^{3/2}} + \mathcal{N}_{2,\text{PB}}^{(\text{NLO})} \frac{\exp\left(-\sqrt{\frac{2}{3}}\kappa L\right)}{(\kappa L)^{5/2}}. \quad (48)$$

We also assume the amplitude to the NLO corrections to be of the size of the leading-order amplitude and again set $\mathcal{N}_{\text{PB}}^{(\text{LO})} = \mathcal{N}_{i,\text{PB}}^{(\text{NLO})}$ in the expressions above.

As discussed in Sec. III, the effects of general twisted boundary conditions in an N-body system are obtained by multiplying the wave function in a box by a phase related to the twists whenever one leaves the box [Eq. (28)],

$$\Delta E_L^{(\text{LO})}(\{\boldsymbol{\phi}_i\}) = \sum_{i=1}^{3} \sum_{(\boldsymbol{n}_i,\boldsymbol{n}_j,\boldsymbol{n}_k)\in M_i} v(\boldsymbol{n}_i,\boldsymbol{n}_j,\boldsymbol{n}_k) e^{i\sum_{l=1}^{3}\boldsymbol{\phi}_l\cdot\boldsymbol{n}_l}.$$

Instead of a factor of $3\times2\times2\times3$ [spatial dimensions $\times$ sign of vector $\times$ permutations of (j,k) for fixed i $\times$ permutations of i] when executing the sum over all neighboring lattice vectors, the restriction $(\boldsymbol{n}_i,\boldsymbol{n}_j,\boldsymbol{n}_k) \in M_i$ [Eq. (27)] reduces the sum to factors involving cosines that depend on the twist angles,[7]

$$\Delta E_L^{(\text{LO})}(L,\{\boldsymbol{\phi}_i\}) = A^{(\text{LO})}(\{\boldsymbol{\phi}_i\}) \frac{\exp\left(-\frac{2}{\sqrt{3}}\kappa L\right)}{(\kappa L)^{3/2}} \quad (49)$$

$$A^{(\text{LO})}(\{\boldsymbol{\phi}_i\}) = \frac{\mathcal{N}_{\text{PB}}^{(\text{LO})}}{9} \sum_{i,j=1}^{3} \cos(\boldsymbol{e}_j\cdot\boldsymbol{\phi}_i). \quad (50)$$

[6]The argument of the wave function gets shifted by one box size in two different directions: $\psi(\boldsymbol{n}) \mapsto \psi(\boldsymbol{n} + (\boldsymbol{e}_1 + \boldsymbol{e}_2)L)$.

[7]It is interesting to study this scenario in the N-body case as well. Because one expects no directional dependence of the leading-order finite-volume energy shift in the unitary limit of N identical bosons, one can assume that the general twist dependence of this shift can be expressed by Eq. (50) when changing 3 to N. We are currently studying the twist dependence in the N-body fermionic case [33].

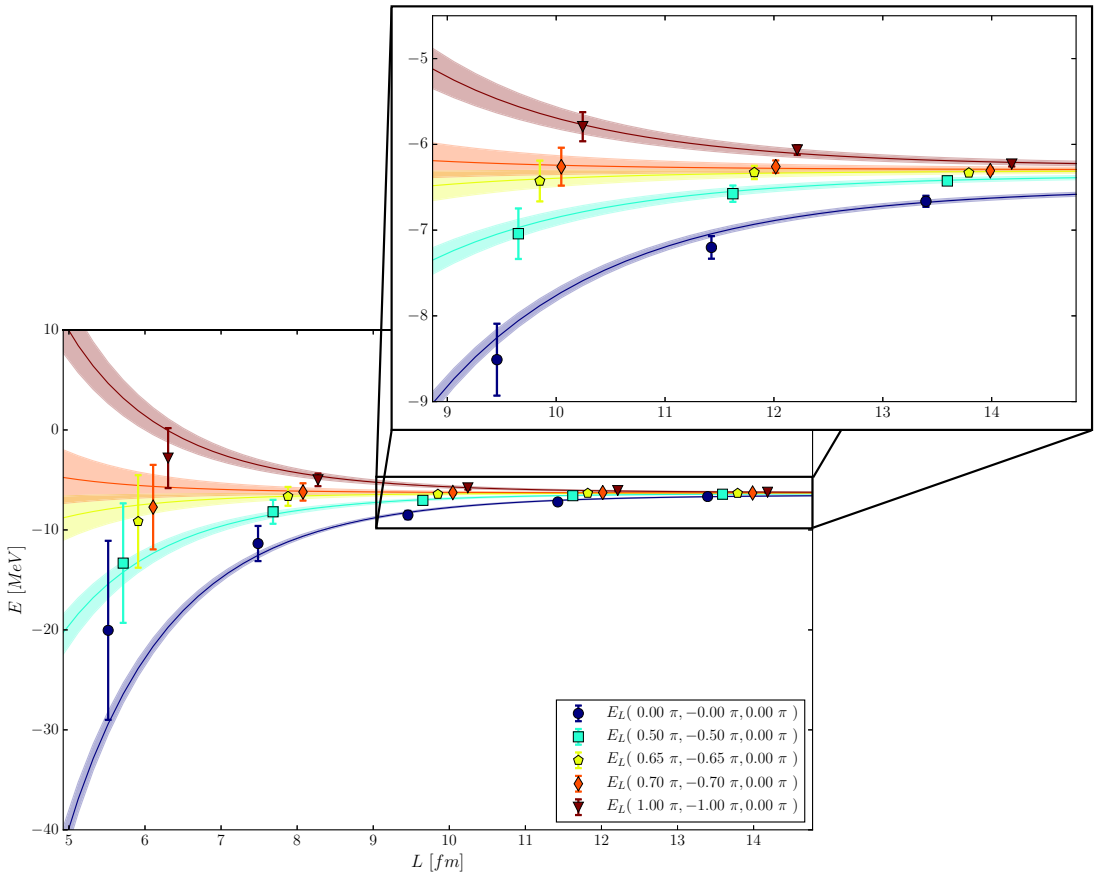

FIG. 7. Individually selected three-body fits for a fit range from $L \approx 6$ to 14 fm, which corresponds to $L = aN_L$ with $a = 1.97$ fm. Extracted infinite-volume energies, amplitudes, and average χ^2 can be extracted from Fig. 8. The error bars and error bands correspond to 1σ. Data points and bands are slightly shifted in the L direction for visualization purposes.

Again, as in the two-body case, we restrict ourselves to equal boosts in each spatial direction $\boldsymbol{e}_j \cdot \boldsymbol{\phi}_i = \phi_i \in [0,2\pi]$ and the sum of all twist angles is constrained to zero to ensure zero c.m. motion. To analyze the twist-angle dependence of the leading-order FV corrections, calculations were performed using three different angle orientations,

$$(\phi_1,\phi_2,\phi_3) = (\phi,-\phi,0), \quad (\phi,\phi,-2\phi), \quad (\phi,2\phi,-3\phi). \quad (51)$$

The number of different computed configurations can be found in Table III, selected energy fits from our calculated distributions are displayed in Fig. 7, and the corresponding amplitudes coming from all our fits as well as their predictions can be found in Fig. 8.

In contrast to the two-body case, the extrapolated infinite-volume energy as well as their average χ^2_{avg} of individual fits depend on the twists, as can be seen by comparing the top and bottom panels of Fig. 8. This is to be expected because we have used in our fits a FV functional form [Eq. (47)] that does not represent our system exactly. Errors in the fitted amplitudes and energies can, and most certainly are, correlated in this case (compare top and center panels of Fig. 8). We can explicitly see how such correlations come about by considering the following example. Let us assume that the exact leading-order FV expression is parametrized by

$$\Delta E^{(\text{LO})}_{L,\text{exact}}(L,\phi) = A^{(\text{LO})}(\phi)\big[\Delta E^{(\text{LO})}_{L,\text{used}}(L,0) + \Delta E^{(\text{LO})}_{L,\text{corr}}(L)\big],$$

where $\Delta E^{(\text{LO})}_{L,\text{used}}(L,0)$ is given by Eq. (47) and $\Delta E^{(\text{LO})}_{L,\text{corr}}(L)$ is its correction. The extracted infinite-volume energy will have an explicit dependence on the twist angles because

$$\begin{aligned} E(L,\phi) &= E_\infty + \Delta E^{(\text{LO})}_{L,\text{exact}}(L,\phi) + \delta E(L) \\ &= E_\infty + A^{(\text{LO})}(\phi)\big[\Delta E^{(\text{LO})}_{L,\text{used}}(L,0) \\ &\quad + \Delta E^{(\text{LO})}_{L,\text{corr}}(L)\big] + \delta E(L) \qquad (52) \\ &= E_\infty + \delta E_\infty(L,\phi) + \Delta E^{(\text{LO})}_{L,\text{used}}(L,\phi) + \delta E(L). \qquad (53) \end{aligned}$$

The expression above shows how errors in the form of the fitting function $\Delta E^{(\text{LO})}_{L,\text{used}}$ can induce twist-angle dependence and correlations $\delta E_\infty(L,\phi)$ on our extrapolated energies E_∞. Comparing Eqs. (52) and (53), we note that as $A^{(\text{LO})}(\phi) \to 0$, one has $\delta E_\infty(L,\phi) \to 0$. Thus, the fitting expression, regardless of form, becomes exact in this limit.

Returning to Fig. 7, we find that the shape of the leading-order FV corrections is similar to that of the two-body deuteron system. In particular, one finds energies converging from below

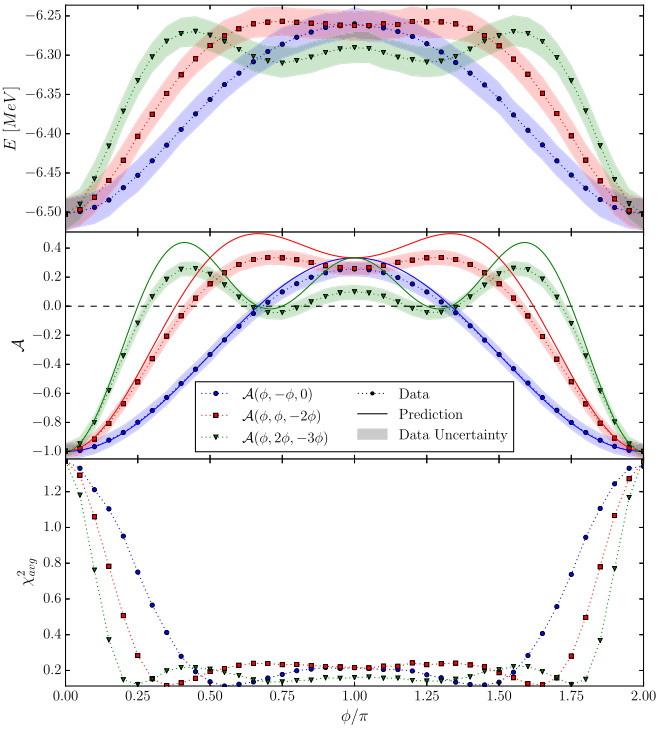

FIG. 8. Triton results for individual twist-fitting procedure. The figure contains the individually extracted infinite-volume energy results (top), the amplitudes of the leading-order FV behavior (center), as well as the average χ^2_{avg} (bottom) for each fit in a fitting range from $L \approx 6$ to 14 fm. The data points are obtained for three different angle configurations (circle, square, triangle). Data points correspond to dots (and are connected via dotted lines), the uncertainties of the data points correspond to the bands, and the solid lines are the predictions for the behavior of the amplitude. The error bands correspond to an 1σ confidence interval of the propagated errors.

and above the infinite-volume energy. However, because of the dimensionality of the problem, the accessible box sizes were not sufficiently large to enter the asymptotic region where the error bands overlap.

The amplitude fits in the center panel of Fig. 8 suggests that certain twist-angle combinations have significantly reduced FV corrections [i.e.. when $\mathcal{A}(\phi) := -A(\phi)/A(0) = 0$], similar to the iPBC case in the two-body system.[8] Indeed, from the predicted shape of the amplitude twist dependence in Eqs. (49) and (50), the three-body analog to iPBCs occurs for twist angles that solve the following equation:

$$\sum_{j=1}^{3} \cos(\boldsymbol{\phi}_1 \cdot \boldsymbol{e}_j) + \cos(\boldsymbol{\phi}_2 \cdot \boldsymbol{e}_j) + \cos[(\boldsymbol{\phi}_1 + \boldsymbol{\phi}_2) \cdot \boldsymbol{e}_j] = 0. \tag{54}$$

[8]The term "i-periodic" in the two-body case refers to angles that produce a purely imaginary phase (i.e., $\theta = \pi/2$) and that also significantly reduce LO FV effects. For the three-body case, we designate the term i-periodic analogs to refer to twist angles that eliminate the leading-order FV effects, but are not, in general, purely imaginary.

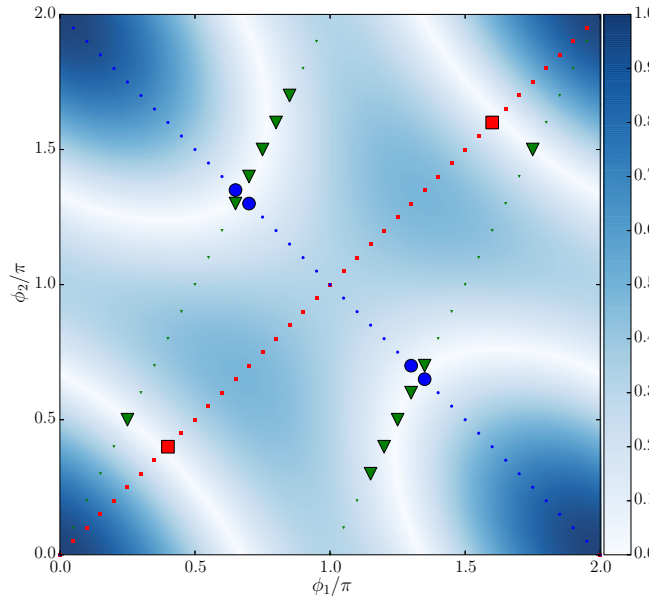

FIG. 9. Contour plot for three-body iPBC analogs. The contour expresses the relative amplitude of the predicted analytic LO FV corrections depending on the twists: $\mathcal{A}^{(\text{LO})}(\phi_1,\phi_2,-\phi_1-\phi_2)$ [Eq. (50)]. The light area corresponds to the solutions for the three-body iPBC analogs: $\mathcal{A}^{(\text{LO})} = 0$ [Eq. (55)] and the points (both large and small) represent the twist angles we have used in our study. The larger points have been identified with the numerically found iPBC analogs extracted from Fig. 8 (see text). As in Fig. 8 the color code represents data for a fixed ratio of ϕ_2/ϕ_1: (circle, square, triangle) = (−1,1,2).

If one twists each spatial direction equivalently, this reduces to

$$\cos(\phi_1) + \cos(\phi_2) + \cos(\phi_1 + \phi_2) = 0. \tag{55}$$

Note that the analog to iPBC twists is not unique in the three-body system, as opposed to the deuteron case. In particular, there is a one-dimensional set of values for ϕ which eliminate the leading-order FV effect. In Fig. 8, for example, the iPBC analog twist angles correspond to the values of ϕ where the solid curves of $\mathcal{A}(\phi) = 0$ (center panel).

As found in the deuteron case, we point out here that our numerical results deviate from their predictions in the regions of higher twist momenta, e.g., for the $\phi_1 = -\phi_2$, $\phi_3 = 0$ (dotted line with circles), this data is inconsistent within errors with the prediction at twist angles around $p_{\phi_1} = 0.8\,\pi/L$. For the $\phi_1 = \phi_2$, $\phi_3 = 2\phi_1$ (dotted line with squares) and the $\phi_2 = 2\phi_1$, $\phi_3 = 3\phi_1$ (dotted line with triangles), the discrepancies are prominent once $p_{\phi_3} = 0.6\,\pi/L$ and $p_{\phi_3} = 0.6\,\pi/L$, respectively. We return to this topic in Sec. VII.

In Fig. 9 we give a contour plot which shows all the allowed iPBC analog twist values for the three-body system investigated in this paper. The contour itself represents the left-hand side of Eq. (55) and thus the predicted relative amplitude of the LO FV corrections. The maximal values correspond to the dark regions (periodic and other boundaries) and the minima to the white regions (i-periodic boundaries). The plain white area corresponds to the solutions of Eq. (55) and the points are the locations of pairs of (ϕ_1,ϕ_2), which

were used for in our numerical investigations. The larger points give the numerically extracted twist angles that are consistent (within errors) with $\mathcal{A}(\phi) = 0$, results which are valid to all orders of the FV corrections. The data points of Fig. 9 use the same color designations as in Fig. 8. The results in the middle panel of Fig. 8 represent cross sections of Fig. 9 along the dotted lines and thus the data points share a 2π periodicity. Similar to the two-body case, we find that a complete averaging of twists does not completely remove FV effects in the three-body system.

VII. COMMENT ON DISCRETIZATION EFFECTS

As already pointed out, we find systematic differences between our numerical results and their predictions in regions of large twist angles $\phi \gtrsim 0.6\pi$, as can be seen from Figs. 3 and 8. Also for the three-body case, owing to the periodicity of the twist angles, one would expect all our numerical results to be equivalent at $\phi = \pi$, in addition to having agreement with their analytic predictions. We now present arguments that show that these discrepancies originate most likely from discretization errors. Consider the following picture of a simple discrete "one-step" derivative in the context of twisted boundary conditions

$$\partial^2_{x,a} f(\boldsymbol{r}) := \frac{1}{a^2}[e^{i\phi_x a/L} f(\boldsymbol{r} + a\boldsymbol{e}_x) - 2f(\boldsymbol{r}) + e^{-i\phi_x a/L} f(\boldsymbol{r} - a\boldsymbol{e}_x)]. \tag{56}$$

If one now computes the expectation value of the momentum operator squared $\langle p^{\phi\,2}_{x,a}\rangle$ for a given wave function ψ and twist angle ϕ, then expands this wave function and rewrites this with the continuum expectation values of the momentum operator for periodic boundaries

$$\langle p^n_x\rangle := \int d^3\boldsymbol{x}\,\psi^*(\boldsymbol{x})\big(-i\partial^n_x\big)\psi(x), \tag{57}$$

one finds that

$$\big\langle p^{\phi\,2}_{x,a}\big\rangle = \langle (p_x + \phi_x/L)^2\rangle - \frac{a^2}{12}\langle (p_x + \phi_x/L)^4\rangle + \mathcal{O}(a^4). \tag{58}$$

As the first term in Eq. (58) can be identified with the continuum limit twist momentum, the expectation value of the momentum operator squared obtains a negative shift for a nonzero lattice spacing. Such a shift scales as $a^2(\phi/L)^2$ plus higher terms for a "single-step" derivative. These results are completely consistent with our findings of a reduced offset in our numerical results for large shift angles, because in our computations the potential was purely local and the only structure actually affected by twists was the kinetic energy operator. Therefore, the total energy of all the computed states experience a shift to more negative values compared to the continuum limit; the larger the twist momentum (modulo periodicity), the larger is the shift. As this effect is most dominant for small boxes and the finite-volume shift exponentially decays as well, the magnitude of the exponential decay is eventually smaller compared to the result in a continuous space. A definitive proof that our offsets are indeed attributable to discretization effects would require calculations performed at smaller lattice spacings, as well as the use of higher-order improved differencing schemes. We are actively investigating this.

VIII. CONCLUSION

In this paper we investigated the effects of twisted boundary conditions on two- and three-body nuclear systems. We performed investigations using the NLEFT formalism, with appropriate modifications to affect twisted boundaries and utilized a simplified NN interaction. We benchmarked our two-body results to known analytic results from Ref. [24], and extended the analysis in the two-body sector to additional twist angles. We performed the same analysis to the three-body (triton) sector, where we derived the three-body iPBC analog quantization condition and numerically verified their corresponding FV cancellations. As opposed to the deuteron case, we found multiple iPBC analog twist possibilities in the three-body sector.

We have attempted a detailed analysis of our fitting and extraction routines, where we enumerate all (known) sources of systematic errors. Where possible, we assign realistic errors or very conservative errors in our error budget. We find that, in both two-body and three-body systems, results obtained with iPBC analogs were superior to twist averaging, under the constraint that the allowed twists preserved zero c.m. motion. In our three-body calculations, we found correlations and twist-angle dependence in our extrapolated binding energies. As we demonstrated, this finding is to be expected because the leading-order FV functional form we used to extract our results was derived for three particles at the unitary limit [17], which does not describe our system exactly.

Our analysis suggests that discretization effects also influence finite-volume effects for nonzero twists. We have provided formal arguments to support this finding, and we intend to do a more detailed analysis of this effect using several lattice spacings as well as more complex A-body systems to confirm this.

Our work also shows that the implementation of twisted boundaries for N-body systems within the NLEFT formalism is, in principle, relatively easily done. One simply has to multiply off-diagonal matrix elements of the transfer matrix by a phase associated with the twists. One might fear that this procedure increases sign oscillations during stochastic computations; however, the corresponding operators remain Hermitian and the eigenvectors and corresponding eigenvalues remain real. Furthermore, though in this case only two-body interactions were considered, this can be easily generalized to N-body interactions.

In this study we applied twists to nucleon degrees of freedom within a nonrelativistic formulation. We found that the iPBC analog twists exactly canceled the leading-order FV effects. This is contrasted to LQCD calculations that employ twists (or partial twists), because here the twists are applied directly to quarks. The interactions in this case can also depend on the twist angles owing to propagation of pions around the torus. As such, we do not expect exact cancellation of

leading-order FV effects, but rather a suppression. It would be interesting to quantify this level of suppression from LQCD studies that utilize our iPBC analog twist-angle condition in Eqs. (54) and (55).

The most intriguing aspect of this work is the demonstration of iPBC analog twists for the three-body sector, which have vastly reduced FV corrections compared to PBCs. This raises the question of whether there exists more general iPBC analog twists for N-body systems. The possibility of iPBC analog twist angles for higher N-body systems would be an important finding for finite-volume numerical simulations because this would allow for calculations in smaller volumes accompanied by their significant reduction in computational costs. Our findings in the three-body sector, coupled with other investigations of more general N-body systems [33,34], provides credence that analogs of iPBC angles exist for nonrelativistic N-body systems in general.

ACKNOWLEDGMENTS

We acknowledge financial support from the Magnus Ehrnrooth Foundation of the Finnish Society of Sciences and Letters, which enabled some of our numerical simulations. We are indebted to S. König, T. Lähde, and A. Shindler for insightful discussions. We thank D. Lee for initial discussions related to applying TBCs within the NLEFT formalism.

[1] S. R. Beane, E. Chang, S. D. Cohen, W. Detmold, H. W. Lin, T. C. Luu, K. Orginos, A. Parreno, M. J. Savage, and A. Walker-Loud (NPLQCD), Light nuclei and hypernuclei from quantum chromodynamics in the limit of SU(3) flavor symmetry, Phys. Rev. D **87**, 034506 (2013).

[2] S. R. Beane, E. Chang, S. D. Cohen, W. Detmold, H. W. Lin, T. C. Luu, K. Orginos, A. Parreno, M. J. Savage, and A. Walker-Loud, Hyperon-Nucleon Interactions and the Composition of Dense Nuclear Matter from Quantum Chromodynamics, Phys. Rev. Lett. **109**, 172001 (2012).

[3] S. R. Beane E. Chang, W. Detmold, B. Joo, H. W. Lin, T. C. Luu, K. Orginos, A. Parreno, M. J. Savage, A. Torok, and A. Walker-Loud (NPLQCD), Evidence for a Bound H-Dibaryon from Lattice QCD, Phys. Rev. Lett. **106**, 162001 (2011).

[4] K. Orginos, A. Parreno, M. J. Savage, S. R. Beane, E. Chang, and W. Detmold, Two nucleon systems at $m_\pi \sim 450$ MeV from lattice QCD, Phys. Rev. D **92**, 114512 (2015).

[5] F. Etminan, H. Nemura, S. Aoki, T. Doi, T. Hatsuda, Y. Ikeda, T. Inoue, N. Ishii, K. Murano, and K. Sasaki (HAL QCD), Spin-2 $N\Omega$ dibaryon from lattice QCD, Nucl. Phys. A **928**, 89 (2014).

[6] T. Inoue, S. Aoki, T. Doi, T. Hatsuda, Y. Ikeda, N. Ishii, K. Murano, H. Nemura, and K. Sasaki (HAL QCD Collaboration), Two-baryon potentials and H-dibaryon from 3-flavor lattice QCD simulations, Nucl. Phys. A **881**, 28 (2012).

[7] T. Yamazaki, K.-i. Ishikawa, Y. Kuramashi, and A. Ukawa, Study of quark mass dependence of binding energy for light nuclei in 2+1 flavor lattice QCD, Phys. Rev. D **92**, 014501 (2015).

[8] T. Yamazaki, K.-i. Ishikawa, Y. Kuramashi, and A. Ukawa, Helium nuclei, deuteron and dineutron in 2+1 flavor lattice QCD, Phys. Rev. D **86**, 074514 (2012).

[9] E. Epelbaum, H. Krebs, D. Lee, and U.-G. Meißner, Lattice effective field theory calculations for $A = 3,4,6,12$ nuclei, Phys. Rev. Lett. **104**, 142501 (2010).

[10] E. Epelbaum, H. Krebs, D. Lee, and U.-G. Meißner, Ab Initio Calculation of the Hoyle State, Phys. Rev. Lett. **106**, 192501 (2011).

[11] E. Epelbaum, H. Krebs, T. A. Lähde, D. Lee, U.-G. Meißner, and G. Rupak, Ab Initio Calculation of the Spectrum and Structure of ^{16}O, Phys. Rev. Lett. **112**, 102501 (2014).

[12] E. Epelbaum, H. Krebs, T. A. Lähde, D. Lee, and U.-G. Meißner, Viability of Carbon-Based Life as a Function of the Light Quark Mass, Phys. Rev. Lett. **110**, 112502 (2013).

[13] T. A. Lähde, T. Luu, D. Lee, U.-G. Meißner, E. Epelbaum, H. Krebs, and G. Rupak, Nuclear lattice simulations using symmetry-sign extrapolation, Eur. Phys. J. A **51**, 92 (2015).

[14] T. A. Lähde, E. Epelbaum, H. Krebs, D. Lee, U.-G. Meißner, and G. Rupak, Lattice effective field theory for medium-mass nuclei, Phys. Lett. B **732**, 110 (2014).

[15] M. Lüscher, Two particle states on a torus and their relation to the scattering matrix, Nucl. Phys. B **354**, 531 (1991).

[16] S. R. Beane, P. F. Bedaque, A. Parreno, and M. J. Savage, Two nucleons on a lattice, Phys. Lett. B **585**, 106 (2004).

[17] U.-G. Meißner, G. Rios, and A. Rusetsky, Spectrum of Three-Body Bound States in a Finite Volume, Phys. Rev. Lett. **114**, 091602 (2015).

[18] N. Byers and C. N. Yang, Theoretical Considerations Concerning Quantized Magnetic Flux in Superconducting Cylinders, Phys. Rev. Lett. **7**, 46 (1961).

[19] M. Guagnelli, K. Jansen, F. Palombi, R. Petronzio, A. Shindler, and I. Wetzorke (Zeuthen-Rome/ZeRo), Continuous external momenta in nonperturbative lattice simulations: A computation of renormalization factors, Nucl. Phys. B **664**, 276 (2003).

[20] P. F. Bedaque and J.-W. Chen, Twisted valence quarks and hadron interactions on the lattice, Phys. Lett. B **616**, 208 (2005).

[21] C. Lin, F. H. Zong, and D. M. Ceperley, Twist-averaged boundary conditions in continuum quantum Monte Carlo, Phys. Rev. E **64**, 016702 (2001).

[22] C. Lehner and T. Izubuchi, Towards the large volume limit - A method for lattice QCD + QED simulations, PoS (**LATTICE2014**), 164 (2015).

[23] B. Schuetrumpf and W. Nazarewicz, Twist-averaged boundary conditions for nuclear pasta Hartree-Fock calculations, Phys. Rev. C **92**, 045806 (2015).

[24] R. A. Briceño, Z. Davoudi, T. C. Luu, and M. J. Savage, Two-Baryon systems with twisted boundary conditions, Phys. Rev. D **89**, 074509 (2014).

[25] M. Lüscher, Volume dependence of the energy spectrum in massive quantum field theories. 1. Stable particle states, Commun. Math. Phys. **104**, 177 (1986).

[26] S. Bour, S. König, D. Lee, H. W. Hammer, and Ulf-G. Meißner, Topological phases for bound states moving in a finite volume, Phys. Rev. D **84**, 091503 (2011).

[27] S. König, D. Lee, and H. W. Hammer, Non-relativistic bound states in a finite volume, Ann. Phys. **327**, 1450 (2012).

[28] S. König, D. Lee, and H. W. Hammer, Volume Dependence of Bound States with Angular Momentum, Phys. Rev. Lett. **107**, 112001 (2011).

[29] S. König, Effective Quantum Theories with Short- and Long-range Forces, dissertation, urn:nbn:de:hbz:5n-33958, University of Bonn, 2013.
[30] D. Lee, Lattice simulations for few- and many-body systems, Prog. Part. Nucl. Phys. **63**, 117 (2009).
[31] E. Epelbaum, H.-W. Hammer, and U.-G. Meißner, Modern theory of nuclear forces, Rev. Mod. Phys. **81**, 1773 (2009).
[32] B. Borasoy, E. Epelbaum, H. Krebs, D. Lee, and U.-G. Meißner, Lattice Simulations for Light Nuclei: Chiral effective field theory at leading order, Eur. Phys. J. A **31**, 105 (2007).
[33] C. Körber (unpublished).
[34] A. Bulgac and M. M. Forbes, Use of the discrete variable representation basis in nuclear physics, Phys. Rev. C **87**, 051301 (2013).